Coupled removal of Rhodamine B and Cu^{2+} by activating persulfate using micron zero-valent iron

Xiaowei Huo, Yunxin Liu, Sijie Liu, Peng Zhou, Haishen Li, Bo Yang, Dan Yang and Yongli Zhang

ABSTRACT

In this study, micron zero-valent iron (ZVI) was used to activate persulfate (PS) for the coupled removal of Rhodamine B (RhB) and Cu^{2+}. It was observed that the removal of RhB could be significantly enhanced with Cu^{2+} compared with that of the case without Cu^{2+}. In addition, the reaction reduced the RhB by 96% within 10 min, and meanwhile reduced the Cu^{2+} by 60% within 120 min. Investigation of the mechanism revealed that, on the one hand, Cu^{2+} species could be turned into Cu^{0} and Cu^{+} species; on the other hand, PS and Cu^{2+} could first accelerate the corrosion of ZVI to release Fe^{2+}. Then, *in situ* generated Cu^{+} and Fe^{2+} further decomposed PS to produce $\cdot SO_4^-$ and ·OH, which could take part in the removal of RhB. In addition, the ZVI/PS/Cu^{2+} system also showed a wider pH working range than the ZVI/PS system. Our study proved that simultaneous removal of heavy metal and organic compound in the ZVI/PS/Cu^{2+} system was feasible.

Key words | Cu^{2+}, oxidation, persulfate, RhB, zero-valent iron

Xiaowei Huo
Yunxin Liu
Sijie Liu
Peng Zhou
Haishen Li
Bo Yang
Yongli Zhang (corresponding author)
College of Architecture & Environment,
Sichuan University,
Chengdu 610065,
China
E-mail: *xyl_scu@126.com*

Dan Yang
Reproductive & Women-Children Hospital,
Chengdu University of TCM,
Chengdu 611137,
China

INTRODUCTION

Dye wastewater, a common type of pollutant, is continuously generated by industries such as those producing rubber, paper, and textiles, which results in environmental and ecological problems all over the world (Ferreira *et al.* 2016; Bilal *et al.* 2017). What is more, Cu^{2+} is commonly found in wastewater as well as in the food chain, which can create severe renal, central, and hepatic nervous system damage and mucosal irritation (Doong *et al.* 2012). Nevertheless, most developed technologies aim to remove single contaminants in water; hence, it is universally acknowledged that methods to remove dyes and Cu^{2+} from water adequately are necessary.

As is well known, in removing dyes from water, many methods have been reported including coagulation, oxidation, biological processes, membrane filtration, electrochemical degradation, and adsorption (Morshedi *et al.* 2013; Fernandez *et al.* 2014; Lin *et al.* 2015; Yang *et al.* 2016; Wei *et al.* 2017). Among them, advanced oxidation processes (AOPs) are favorable in dye water pollution control because of their superior performance and efficiency (Sharma *et al.* 2015). Nowadays, persulfate (PS) has drawn much attention from researchers due to its high oxidation potential ($E^0 = 2.01$ V) and higher stability and solubility at room temperature (Liang *et al.* 2004; Zhou *et al.* 2013). Vicente *et al.* (2011) reported that the non-selective and high redox potential sulfate radical ($\cdot SO_4^-$, $E^0 = 2.6$ V) by the activation of PS is similar to ·OH. In addition to dye removal, several technologies, including adsorption, ion exchange, chemical precipitation, and electrolysis, have been developed to remove Cu^{2+} from wastewater (Yueming *et al.* 2008; Doong *et al.* 2012).

PS can be activated to generate $\cdot SO_4^-$ by transition metals (Peng *et al.* 2018, 2019). As a typical transition metal, iron has been widely studied because it is inexpensive, effective, and environmentally friendly. Previous studies (Mcelroy & Waygood 1990; Liang *et al.* 2007; Triszcz

doi: 10.2166/aqua.2019.072

et al. 2009; Pulicharla et al. 2018) reported that ZVI and Fe^{2+} were good activators of PS for generating reactive radicals such as $\cdot SO_4^-$ and ·OH (Equations (1)–(3)). Moreover, Fe^{2+} generating and Fe^{3+} recycling (Equation (4)) occur on the ZVI surface, and Cu^{2+} can also be removed by ZVI exchange (Equation (5)). Therefore, using ZVI for the coupled removal of Cu^{2+} and dyes has great potential.

$$S_2O_8^{2-} + Fe^0 \rightarrow Fe^{2+} + SO_4^{2-} \quad (1)$$

$$S_2O_8^{2-} + Fe^{2+} \rightarrow Fe^{3+} + \cdot SO_4^- + SO_4^{2-} \quad (2)$$

$$\cdot SO_4^- + H_2O \rightarrow \cdot OH + H^+ + SO_4^{2-} \quad (3)$$

$$Fe^{3+} + Fe^0 \rightarrow Fe^{2+} \quad (4)$$

$$Cu^{2+} + Fe^0 \rightarrow Fe^{2+} + Cu \quad (5)$$

In this work, RhB and Cu^{2+} were selected as the targets. Our study mainly focuses on: (1) comparing the ZVI/PS system and ZVI/PS/Cu^{2+} system; (2) investigating the removal of Cu^{2+} and/or RhB in the ZVI/PS/Cu^{2+} system under different conditions; (3) identifying the radical species in the ZVI/PS system; (4) analyzing the mechanism of the simultaneous removal of Cu^{2+} and RhB.

MATERIALS AND METHODS

Materials and reagents

All reagents and chemicals were of analytical reagent grade and were used as received, without further purification. The water used for the preparation of the reagents and reaction system was purified by a Milli-Q (18.25 MΩ·cm) system. The solution pH was adjusted by H_2SO_4 and NaOH solution. Micron scale zero-valent iron powder (ZVI, ≥99.9%), sodium persulfate (PS, ≥99%), 5,5-dimethyl-1-pyrrolidine-N-oxide (DMPO, ≥97%), potassium iodide (≥99.0%), and neocuproine hemihydrate (NP, ≥98%) were purchased from Sigma-Aldrich Co., Ltd (Shanghai, China). Rhodamine B (RhB, ≥99%), sulfuric acid (H_2SO_4, analytical grade), sodium hydroxide (NaOH, analytical grade), L-ascorbic acid, tert-butyl alcohol, ethanol, sodium bicarbonate, potassium iodide, and 1,10-phenanthroline were obtained from Kelong Chemical Co., Ltd (Chengdu, China).

Experimental procedures

Twenty-five mg of ZVI was immersed in a beaker (250 mL) with a total solution volume of 250 mL of ultrapure water containing 20 mg/L RhB (and/or 0.02 mmol/L Cu^{2+}, and/or 1.0 mmol/L PS). The mixture was stirred at a constant rate (500 r/min) for 60 min under 25 ± 1 °C condition, then the solution was filtered by a micro PES membrane (pore size: 0.22 μm). The initial reaction time was defined at the moment when ZVI and PS were added. The samples were withdrawn from the reaction solution and the residual samples' concentration in the filtered solution was determined using UV-visible spectrophotometer. The experiments were conducted in air condition. Control experiments were conducted and excluded the interaction between the filter and RhB. All experiments were conducted twice.

Analytical methods

The pH values of solutions were measured by a pH-meter (FiveEasy Plus, Mettler-Toledo, Shanghai). A UV-visible spectrophotometer (UV-1100, Shanghai Mapada Instrument Co., Ltd) was used for analyzing the dye concentrations by measuring the maximum absorbance at a wavelength of 554 nm for RhB. After filtration with a cellulose ester membrane of 0.45 μm pore size and freeze vacuum drying in turn, the solid samples of residual ZVI after the reaction (reaction time 60 min) were prepared. The morphologies and elemental compositions of the ZVI samples before and after oxidation were investigated by a field emission scanning electron microscope (SEM, FEI Inspect F50(FSEM)) equipped with an energy dispersive X-ray spectrometer (EDX, FEI Inspect F50 (FSEM)). X-ray diffraction (XRD, Bruker D8 ADVANCE A25X, Germany) and X-ray photoelectron spectroscopy (XPS, Escalab 250Xi) were also characterized. Electron paramagnetic resonance (EPR) was performed to detect ·OH and $\cdot SO_4^-$, with DMPO as the spin-trapping agents. The ESR spectrum was measured under the following conditions: a center field of 3,505.40 G, a sweep width of 150.00 G, a microwave frequency of 9.84 GHz, a microwave attenuator of 20.00 dB, a microwave power of 2.00 mW, and a sweep time of 10.53 seconds. A multi N/C 3100 analyzer (Analytikjena) was employed to analyze the total organic carbon (TOC).

The concentration of PS was tested by the iodometric titration method using a UV-vis spectrometer (Mapada UV-1100). 0.1 g sodium bicarbonate, 0.5 g potassium iodide, and 4.75 mL Milli-Q water were mixed to create a stock solution, then 0.25 mL of the filtered PS sample was added to stock solution. After 20 min, the concentration of PS was detected by a UV-vis spectrometer at 352 nm (Zhou *et al.* 2017).

The total concentration of dissolved copper (dissolved iron) was determined using a UV-vis spectrometer (Mapada UV-1100). The 2 mL filtered sample, 0.8 mL 0.1 M L-ascorbic acid, 0.4 mL 10 mM NP (0.8 mL 10 mM 1,10-phenanthroline), and 6.8 mL (6.4 mL) of Milli-Q water were mixed to create the Cu^{+}–NP ($[Fe(phen)_3]^{2+}$) complex solution. The concentration of dissolved copper (dissolved iron) was detected by a UV-vis spectrometer at 454 nm (510 nm) (Zhou *et al.* 2017).

RESULTS AND DISCUSSION

Enhancement of ZVI-Cu^{2+} on RhB degradation by activating PS

Experiments were conducted to examine the degradation efficiency of RhB by the ZVI/PS/Cu^{2+} system. As shown in Figure 1, we can see that 25.9% RhB was removed within 60 min in the ZVI system. Fe^0 can induce the chain reactions of oxygen species in oxygenated water to generate several reactive oxygen species, such as $O_2{\cdot}^-$, H_2O_2, $\cdot HO_2$, and ·OH (Equations (6)–(16)) (Liu *et al.* 2019), which can effectively degrade RhB. However, it could be noted that RhB removal was significantly decreased with the addition of Cu^{2+}, which may be because more Fe^0 reacted with Cu^{2+} by ion exchange (Equation (5)). Moreover, RhB was effectively degraded by PS (1.0 mM) in the presence of ZVI (100 mg/L) and Cu^{2+} (0.2 mM), in which more than 15% RhB was degraded by the ZVI/PS system after 10 min. In other words, the reaction rate was higher. Zhou *et al.* (2017) reported that PS could be activated by Cu^{2+} for generating $\cdot SO_4^-$. Remarkably, the RhB removal rate was 0.326 min^{-1} ($R^2 = 0.9484$) and 0.168 min^{-1} ($R^2 = 0.9942$) in the system of ZVI/PS/Cu^{2+} and ZVI/PS, respectively. Control experiments showed that the abatements of PS were negligible.

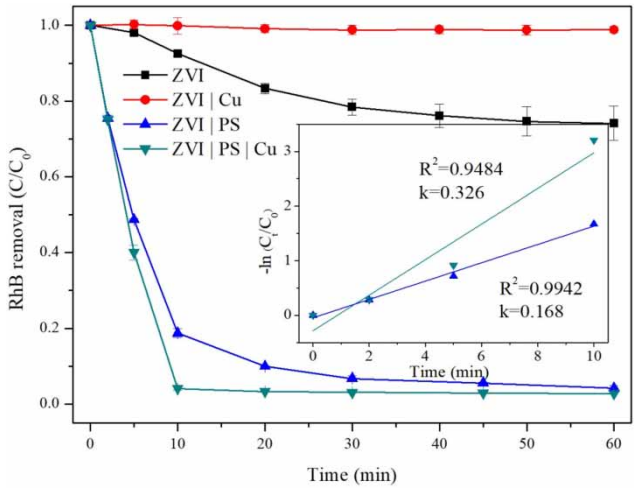

Figure 1 | Enhancement of RhB removal in the ZVI/PS/Cu^{2+} system ($[RhB]_0 = 20$ mg/L, $T = 25 \pm 1$ °C, $[ZVI]_0 = 100$ mg/L, $[PS]_0 = 1.0$ mM, $[Cu^{2+}]_0 = 0.2$ m mM).

In addition, it was found that 60.1% of the Cu^{2+} was removed in the ZVI/PS/Cu^{2+} system. In contrast, compared to the case of ZVI alone, the removal of Cu^{2+} increased to around 73.2%.

$$Fe^0 + 2H^+ + O_2 \rightarrow Fe^{2+} + H_2O_2 \quad (6)$$

$$Fe^0 + H_2O_2 + 2H^+ \rightarrow Fe^{2+} + 2H_2O \quad (7)$$

$$Cu^+ + S_2O_8^{2-} \rightarrow Cu^{2+} + SO_4^{2-} + \cdot SO_4^- \quad (8)$$

$$Fe^{2+} + H_2O_2 \rightarrow Fe^{3+} + \cdot OH + OH^- \quad (9)$$

$$Fe^{3+} + H_2O_2 \rightarrow Fe^{2+} + \cdot HO_2 \quad (10)$$

$$2 \cdot HO_2 \rightarrow H_2O_2 + O_2 \quad (11)$$

$$\cdot HO_2 \leftrightarrow \cdot O_2^- + H^+ \quad (12)$$

$$Fe^{3+} + \cdot HO_2 \rightarrow Fe^{2+} + O_2 + H^+ \quad (13)$$

$$Fe^{3+} + \cdot O_2^- \rightarrow Fe^{2+} + O_2 \quad (14)$$

$$2 \cdot OH \rightarrow H_2O_2 \quad (15)$$

$$\cdot OH + H_2O_2 \rightarrow \cdot HO_2 + H_2O \quad (16)$$

Characterization

To investigate the morphologies and structures of ZVI before and after reaction in the ZVI/PS system and ZVI/PS/Cu^{2+} system, the spectroscopy SEM-EDS were characterized. As shown in Figure 2(a) and 2(b), it can be seen that after the

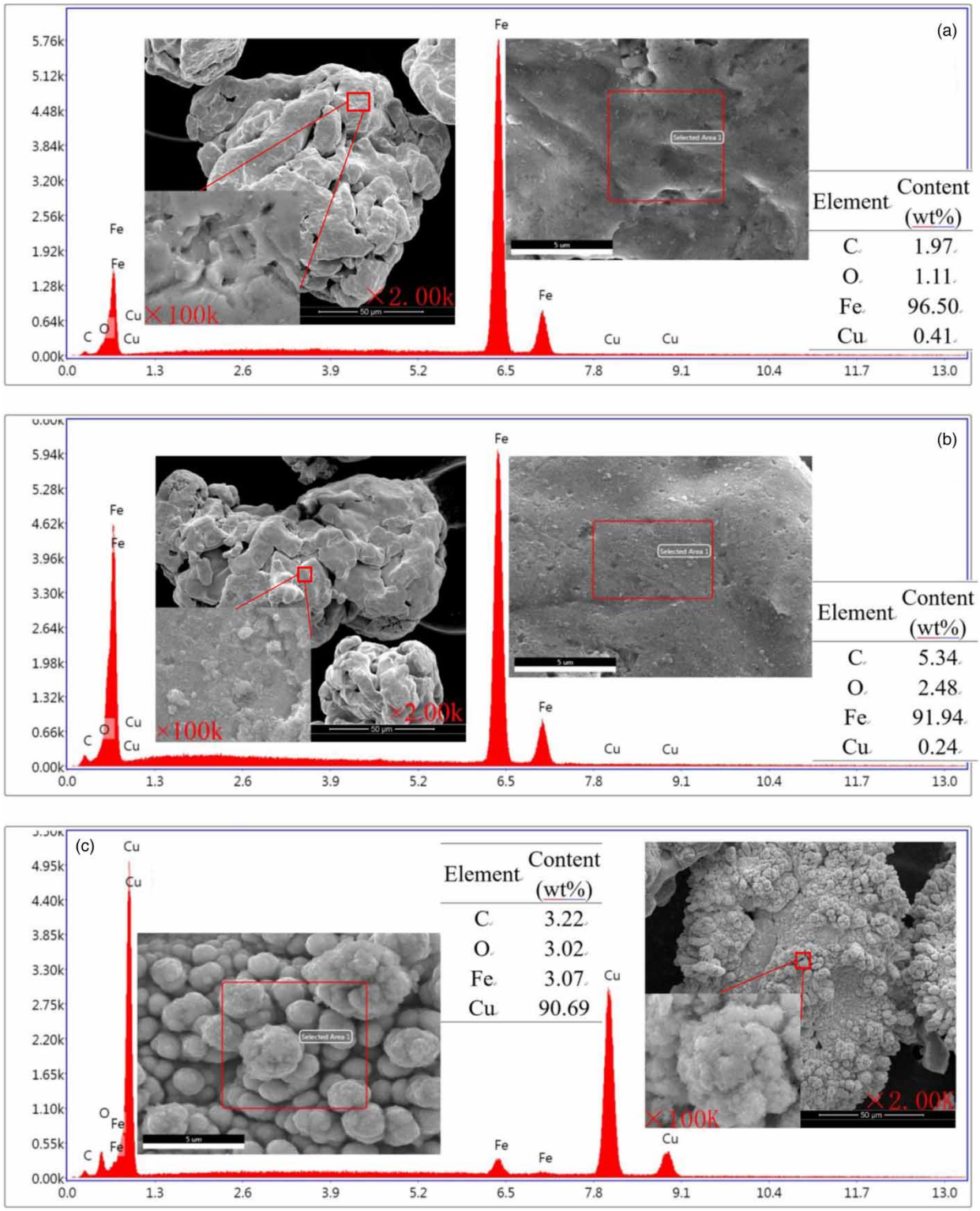

Figure 2 | SEM image and EDS results of ZVI: (a) before reaction, (b) after reaction in the ZVI/PS system, and (c) the ZVI/PS/Cu^{2+} system ($[RhB]_0 = 20$ mg/L, $T = 25 \pm 1$ °C, $[ZVI]_0 = 100$ mg/L, $[PS]_0 = 1.0$ mM, $[Cu^{2+}]_0 = 0.2$ mM).

corrosion of PS, the residual ZVI was rougher than the pristine ZVI powder. Figure 2(c) shows that there are a great deal of spheroidal particles in the ZVI surface areas after reaction of the ZVI/PS/Cu^{2+} system, which is attributed to the generated zero-valent copper (ZVC) (Zhou *et al.* 2017). The EDS result also showed that the ZVI surface contained a large amount of copper, approximately 90%, which indicated that metallic copper was generated and integrated into the ZVI. The EDS results are consistent with the analysis obtained from the SEM analysis.

XRD patterns for the three samples are shown in Figure 3. The characteristic peaks of the pristine ZVI and ZVI after ZVI/PS system and ZVI/PS/Cu^{2+} system reaction powder at 44.7°, 65.3°, and 82.5° matched well with the standard patterns of Fe^0 (PDF#06-0696) (Li *et al.* 2015). The strongest diffraction peaks of the ZVI after ZVI/PS/Cu^{2+} system reaction at 43.3°, 50.4°, and 74.1° also matched well with the standard pattern of Cu^0 (JCPDS-PDF#04-0836) (Zhou *et al.* 2017). Figures 3 and 4(d) indicated that most of the Cu^{2+} species were converted into CuO and Cu^0 after reaction.

XPS was used to further investigate the detailed chemical states and the chemical composition of the ZVI powder before and after reaction in the ZVI/PS system and the ZVI/PS/Cu^{2+} system. The atomic percentages of Fe, O, and Cu elements on the surface of three composites are shown in Table 1 and the XPS survey of the three composites is shown in Figure 4(a), and mainly indicates the presence of Fe 2p, O 1s and Cu 2p signals. Figure 4(b) presents the core level of Fe 2p spectras which can be decomposed into two peaks at 724.1 and 710.6 eV, belonging to 2p1/2 and 2p3/2 binding energies of Fe^{2+} and Fe^{3+} on the ZVI surface (Du *et al.* 2016; Lü *et al.* 2019). As demonstrated in Figure 4(c), the O 1 s peaks at 532.3, 531.1, and 529.5 eV correspond to H_2O or other oxidized iron, OH^- and O^-, respectively (Wu *et al.* 2013). With respect to the areas of the spectra, the amount of Fe 2p and O^- increased after reaction in the ZVI/PS system, and we can conclude that the original ZVI was oxidized in the open air, and more ZVI was oxidized to oxidized iron after the reaction. Conversely, the amount of Fe 2p and O^- or other oxidized iron decreased under the reaction of the ZVI/PS/Cu^{2+} system, and this decrease resulted in generating Cu^0 and CuO. The results in Figure 4(d) indicated that Cu^0 and CuO were detected on ZVI surface. To be specific, the Cu 2p peaks at 954.0 and 934.0 eV represent the binding energy of Cu 2p3/2 and Cu 2p1/2 of Cu^0, and the other peaks located at 962.6, 955.2, 942.5 eV, and 935.0 eV are attributed to CuO on the surface of ZVI powders (Zhou *et al.* 2017). Thereby, it is further confirmed that the Cu^{2+} was removed together with removing RhB.

Table 1 | Atomic percentages of Fe, O, and Cu elements on the surface of three composites obtained from XPS analysis

Element	ZVI	ZVI/PS-after	ZVI/PS/Cu^{2+}-after
Fe (%)	36.49	36.02	17.98
O (%)	63.51	63.98	66.69
Cu (%)	–	–	15.33

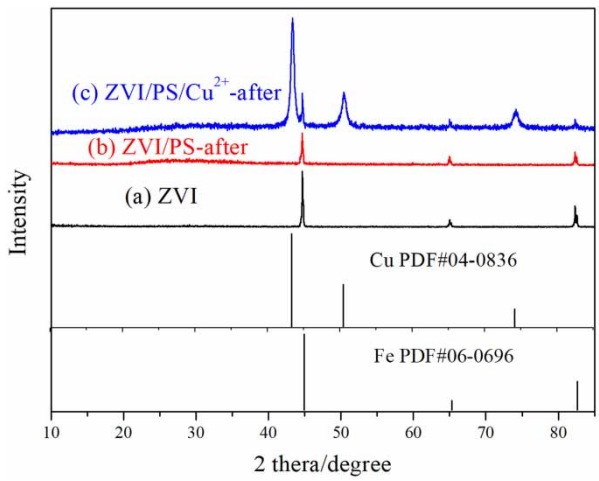

Figure 3 | XRD patterns of the ZVI: (a) before reaction, (b) after reaction in the ZVI/PS system, and (c) the ZVI/PS/Cu^{2+} system ($[RhB]_0 = 20$ mg/L, $T = 25 \pm 1$ °C, $[ZVI]_0 = 100$ mg/L, $[PS]_0 = 1.0$ mM, $[Cu^{2+}]_0 = 0.2$ mM).

Effects of ZVI dosages

The increased ZVI dosage from 20 to 160 mg/L on the removal of RhB and Cu^{2+} in the ZVI/Cu^{2+} system and ZVI/PS/Cu^{2+} system were investigated. In the ZVI/Cu^{2+} system, a higher dosage of ZVI was beneficial in removing Cu^{2+} (Figure 5(c)), but not RhB (Figure 5(a)), which suggests that without PS, the removal rates of RhB were negligible. However, ZVI loading posed significant impacts on the removal of Cu^{2+} and RhB in the ZVI/PS/Cu^{2+} system (Figure 5(b) and 5(c)). The curves between logarithms of

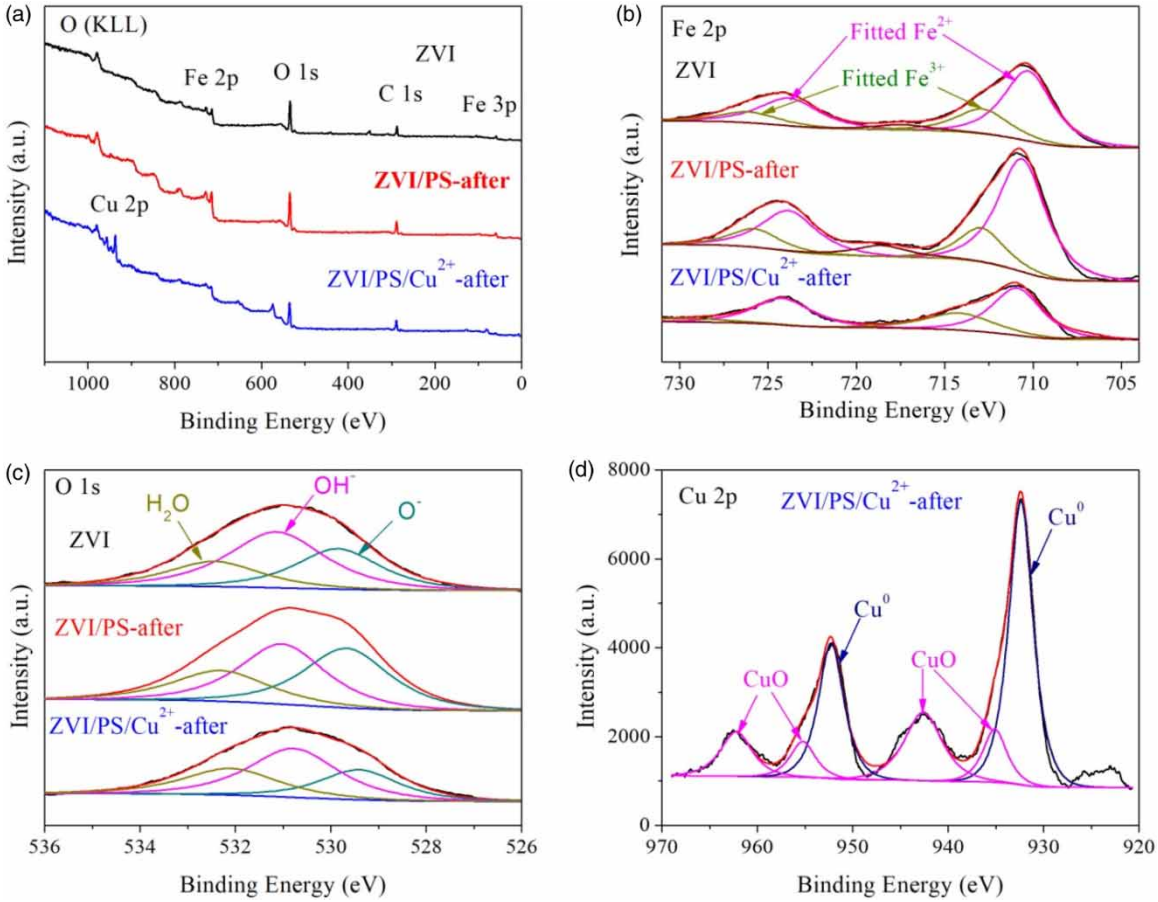

Figure 4 | XPS survey spectra (a), and high resolution XPS spectra for Fe 2p (b), O 1 s (c), and Cu 2p (d) of the ZVI before and after reaction ($[RhB]_0 = 20$ mg/L, $T = 25 \pm 1$ °C, $[ZVI]_0 = 100$ mg/L, $[PS]_0 = 1.0$ mM, $[Cu^{2+}]_0 = 0.2$ mM).

C/C_0 (RhB) and time were plotted in the different ZVI dosage systems, and showed good linearity between C/C_0 and time ($R^2 = 0.9976$, 0.9713, 0.9378, 0.9951, and 0.9871 for the ZVI dosage of 20, 40, 80, 120, and 160 mg/L, respectively). The slopes of C/C_0 against time were estimated to be 0.040, 0.089, 0.289, 0.301, and 0.322, respectively, which can be taken as the orders of reactivity in the RhB removal rates. Further, the higher removal of Cu^{2+} reached 81.0% in the ZVI/PS/Cu^{2+} system.

Effects of Cu^{2+} concentration

Figure 6(a) indicates that the reaction between ZVI-Cu^{2+} and RhB without PS could be neglected, which is consistent with the analysis obtained from Figure 6(a). As shown in Figure 6(b), it is observed that the removal of RhB could also be enhanced slightly when the concentration of Cu^{2+} increased, but the removal rate constants were all higher than those in the ZVI/PS system (data not shown). Figure 6(c) revealed the slight variation in Cu^{2+} degradation rate with raising the initial concentration of Cu^{2+}. On the other hand, Figures 5(c) and 6(c) show a slight decrease in degradation efficiency of Cu^{2+} in the ZVI/PS/Cu^{2+} system compared to the ZVI/Cu^{2+} system. However, these results also clearly demonstrate that the simultaneous removal of RhB and Cu^{2+} can be successfully achieved in the ZVI/PS/Cu^{2+} system.

Effects of pH

There is no doubt that the solution pH plays a significant role in the oxidation process and pH is important for the

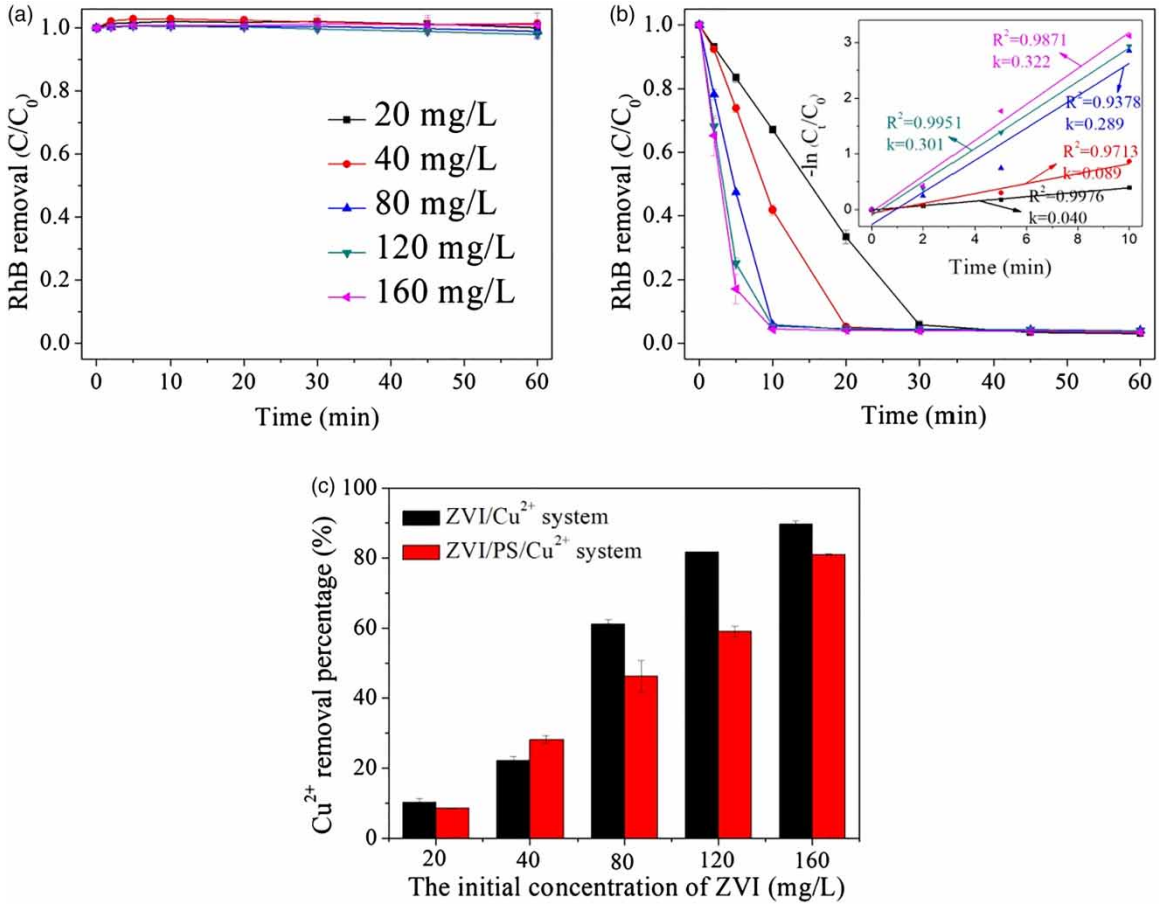

Figure 5 | Effect of ZVI dosage on RhB degradation in the ZVI/Cu^{2+} (a) and ZVI/PS/Cu^{2+} (b) system and Cu^{2+} degradation in the ZVI/Cu^{2+} and ZVI/PS/Cu^{2+} system (c) ($[RhB]_0 = 20$ mg/L, $T = 25 \pm 1°C$, $[ZVI]_0 = 20–160$ mg/L, $[PS]_0 = 1.0$ mM, $[Cu^{2+}]_0 = 0.2$ mM).

lifetime and reactivity of ZVI in water. The effect of initial pH on the removal of RhB by the ZVI/PS system and the simultaneous removal of RhB and Cu^{2+} in the ZVI/PS/Cu^{2+} system are shown in Figure 7. Figure 7(a) and 7(c) show that the lowest initial pH can effectively enhance the RhB removal rate and accelerate the process to reach a steady-state condition within a shorter reaction time. When pH reaches as high as neutral, the RhB removal efficiency drops drastically. Moreover, it is noted that in the same pH conditions, the RhB removal and its removal rate constants in the ZVI/PS/Cu^{2+} system were far superior to that in the ZVI/PS system. As we know, the released Fe^{2+} during the corrosion of ZVI is the main effective iron species to activate PS to produce ·OH and $·SO4^-$ in the ZVI/PS system and the Fe^{2+} can be released in low pH acidic conditions (Equation (6)). However, Cu^{2+} can accelerate the corrosion of ZVI to release Fe^{2+} under higher pH acidic conditions because of ion exchange (Equation (5)) in the ZVI/PS/Cu^{2+} system, which showed a wider pH working range. The Cu^{2+} removal rates also showed a slight change when the pH increases from acidic to neutral conditions.

Proposed mechanism

It is universally acknowledged that $·SO4^-$ and ·OH can be produced via catalyzing PS by ZVI. In this study, the effects of radical scavengers, including ter-butanol and ethanol, were used to investigate the presence of ·OH and $·SO4^-$. Ter-butanol as a scavenger for ·OH exhibited little effect on RhB degradation in the ZVI/PS system and ZVI/PS/Cu^{2+}

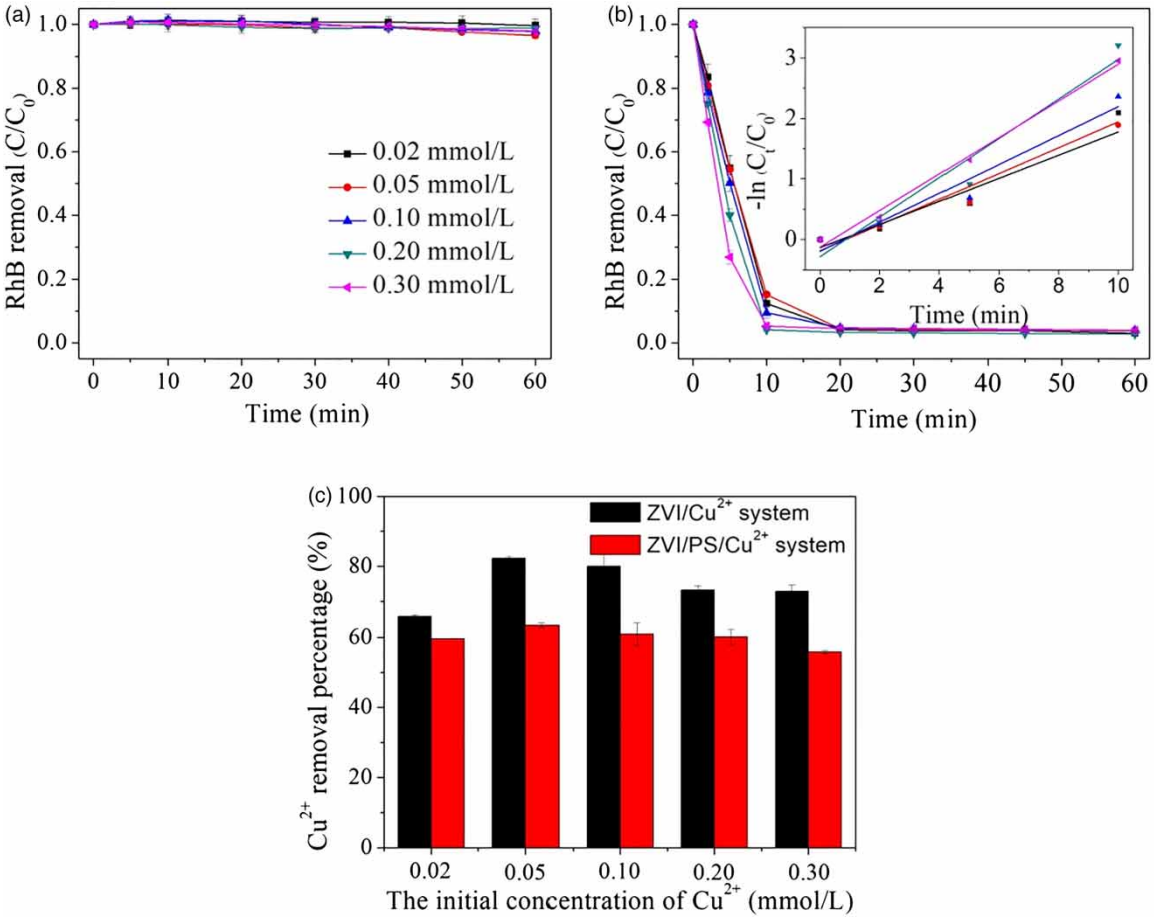

Figure 6 | Effect of Cu^{2+} concentration on RhB degradation in the ZVI/Cu^{2+} (a) and ZVI/PS/Cu^{2+} (b) system and Cu^{2+} degradation in the ZVI/Cu^{2+} and ZVI/PS/Cu^{2+} system (c) ($[RhB]_0 = 20$ mg/L, $T = 25 \pm 1$°C, $[ZVI]_0 = 100$ mg/L, $[PS]_0 = 1.0$ mM, $[Cu^{2+}]_0 = 0.02$–0.3 mM).

system. As shown in Figure 8(a) and 8(b), the removal of RhB was significantly inhibited in the presence of ethanol, which is a scavenger for both ·OH and ·SO4$^-$. It is confirmed that both ·OH and ·SO4$^-$ existed in the ZVI/PS system and ZVI/PS/Cu^{2+} system, indicating that the ·OH and ·SO4$^-$ was likely generated in the reactions between PS and ZVI/Cu^{2+}.

More specifically, EPR spectroscopy, with the spin-trapping reagent of DMPO, was conducted to directly detect the generation of ·OH and ·SO4$^-$. In our study, as shown in Figure 8(c), ·OH and ·SO4$^-$ were quickly produced in the first 2 min.

Based on the results mentioned above, a reaction mechanism for the simultaneous removal of RhB and Cu^{2+} by the ZVI/PS/Cu^{2+} system is proposed in Figure 9.

For the Cu^{2+} removal process, on the one hand, Cu^{2+} species can be reduced into Cu^0 by ion exchange (Equation (5)); on the other hand, Cu^{2+} species can be turned into Cu^+ species via Equations (17) and (18) (Zhou *et al.* 2017; Liu *et al.* 2018). As for the RhB removal process, the PS and Cu^{2+} could first accelerate the corrosion of ZVI, leading to the release of Fe^{2+}; meanwhile, PS could be activated by Cu^+ for generating ·SO4$^-$ (Equation (19)) (Zhou *et al.* 2017), which then dramatically degraded RhB.

$$Fe^0 + 2Cu^{2+} + 2H_2O \rightarrow Fe^{2+} + Cu_2O + H^+ \quad (17)$$

$$2Cu^0 + S_2O_8^{2-} \rightarrow 2Cu^+ + 2SO_4^{2-} \quad (18)$$

$$Cu^+ + S_2O_8^{2-} \rightarrow Cu^{2+} + SO_4^{2-} + \cdot SO_4^- \quad (19)$$

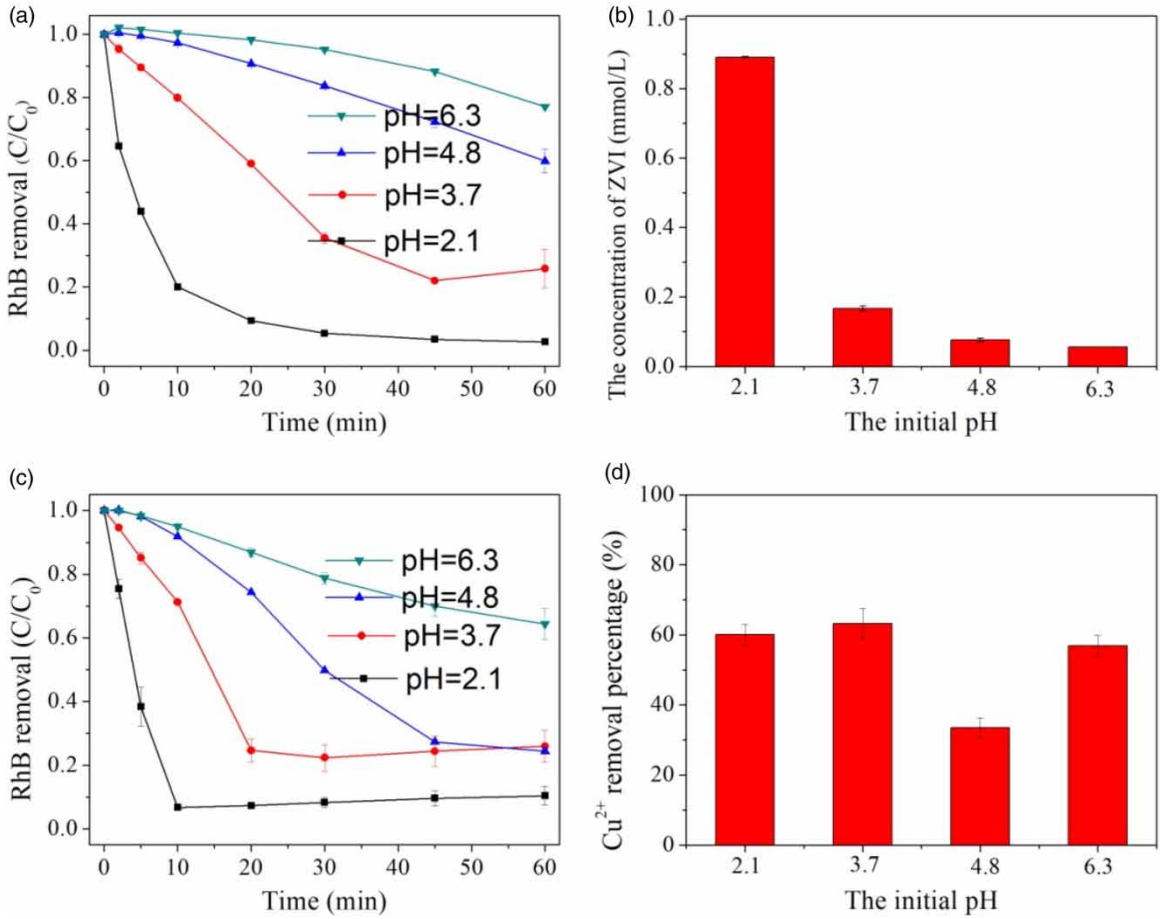

Figure 7 | Influence of initial pH on (a) RhB degradation in the ZVI/PS system, (b) the concentration of ZVI in the solution after 120 min, (c) RhB degradation, and (d) Cu^{2+} removal in the ZVI/PS/Cu^{2+} system ($[RhB]_0 = 20$ mg/L, $T = 25 \pm 1$ °C, $[ZVI]_0 = 100$ mg/L, $[PS]_0 = 1.0$ mM, $[Cu^{2+}]_0 = 0.2$ mM).

Effects of water matrices

The effectiveness of the oxidative process might be affected by the composition of the raw water, and the effects of water matrices on the RhB and Cu^{2+} removal by the ZVI/PS/Cu^{2+} system are illustrated in Figure 10. The water samples were collected at Sichuan University. Table 2 displays the characteristics of five water samples. Apparently, the oxidative efficiency of RhB in deionized water (DW, 95.9%, within 10 min reaction) was much higher than in running water (RW, 92.9%, within 30 min reaction), Jiang'an River water (JAW, 88.5%, within 30 min reaction), Mingyuan Lake water (MYW, 74.7%, within 45 min reaction), and landscape water (LW, 76.1%, within 45 min reaction). As shown in Figure 10(b), it is notable that the TOC removal efficiency of RhB in DW (36.4%) was much higher than those in RW (13.3%), JAW (6.4%), MYW (18.8%), and LW (10.8%). Interestingly, an opposite effect on the Cu^{2+} removal rate was found in the water matrices. Nearly 95.8, 82.4, 60.1, and 92.5% of Cu^{2+} removal rates were found at the water matrices of RW, JAW, MYW, and LW, respectively, which were all higher than that in DW (60.1%).

There may be some reasons for that, on the one hand, the removal of RhB and TOC were inhibited in actual water which was probably because of the higher pH and the natural dissolved organic matters and inorganic species in actual water, especially the high TOC levels. The main constituents of TOC are involved in hydrophobic, transphilic, and hydrophilic DOCs (Vigneswaran 2006; Oh *et al.* 2017; Hu *et al.* 2018), where they can compete with RhB for reactive radicals. On the other hand, because the

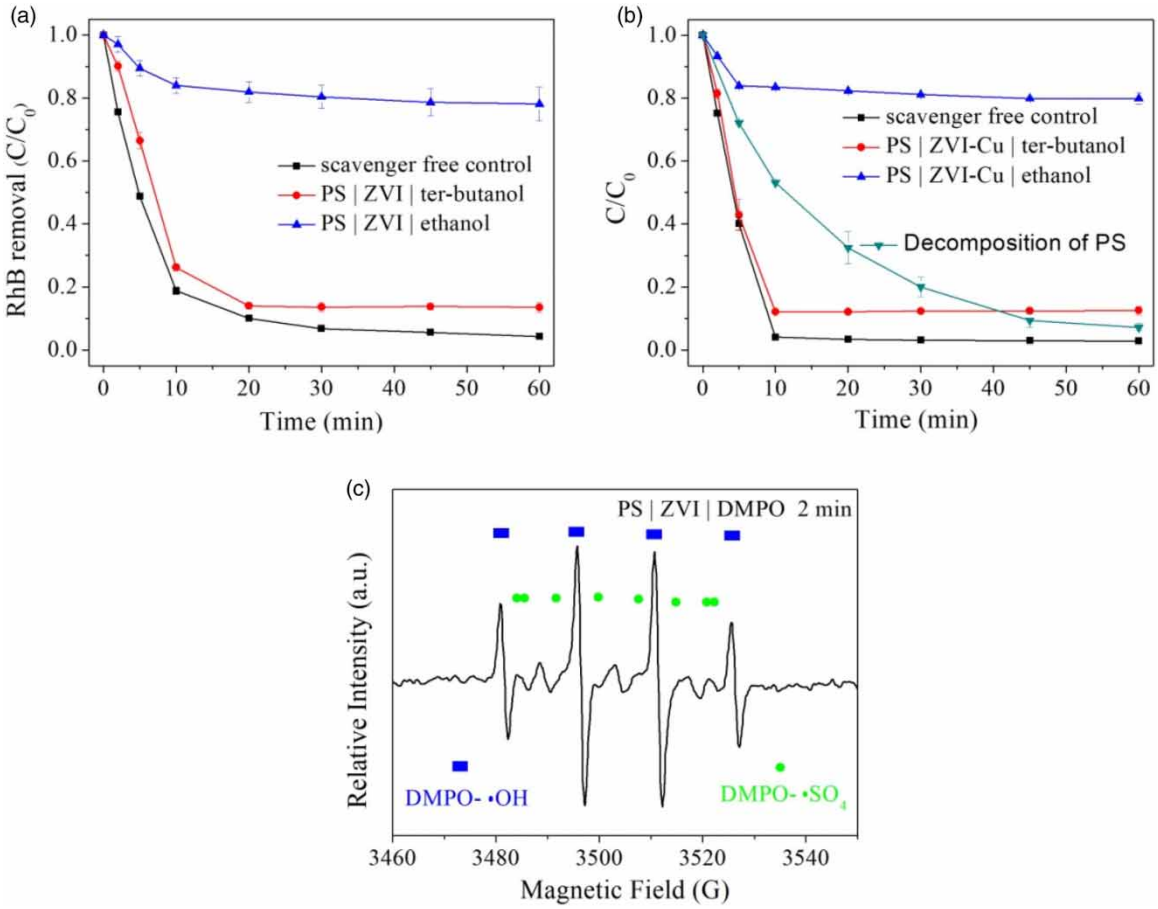

Figure 8 | (a) Effect of scavengers on RhB degradation in the ZVI/PS system and ZVI/PS/Cu^{2+} system for ter-butanol and ethanol. (b) Decomposition of PS in the presence of ZVI and Cu^{2+}. (c) EPR spectra of DMPO-·OH and DMPO-·SO_4^- adduct (DMPO) formed in aqueous solution containing PS, ZVI, and DMPO ($[RhB]_0 = 20$ mg/L, $T = 25 \pm 1$ °C, $[ZVI]_0 = 100$ mg/L, $[PS]_0 = 1.0$ mM, $[ter\text{-}butanol]_0$ and $[ethanol]_0 = 0.1$ M, $[Cu^{2+}]_0 = 0.2$ mM).

oxidative efficiency of RhB was much lower, for the same amount of ZVI, there was more ZVI to remove Cu^{2+}.

All in all, for real water bodies, all water samples showed a decrease in the degradation efficiency of RhB but a distinctly increased effect on Cu^{2+} removal. Nevertheless, the present ZVI/PS/Cu^{2+} system showed great potential to get rid of the RhB and Cu^{2+} wastewater.

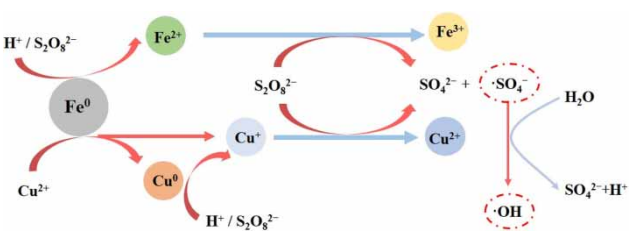

Figure 9 | Proposed reaction mechanism for the synergistic reduction of Cu^{2+} and oxidation of RhB by the ZVI/PS/Cu^{2+} system.

CONCLUSIONS

In our study, we have demonstrated the simultaneous removal of RhB and Cu^{2+} in the ZVI/PS/Cu^{2+} system under acidic conditions. It was clearly shown that Cu^{2+} could enhance the removal of RhB in the ZVI/PS/Cu^{2+} system. A high reactivity towards the coupled removal of RhB and Cu^{2+} was successfully achieved in the ZVI/PS/Cu^{2+} system. Furthermore, the RhB removal increased with higher ZVI and lower pH, but had little impact on the Cu^{2+} concentration. Investigation of the mechanism revealed that the main free radicals produced from the ZVI/PS/Cu^{2+} system were ·SO_4^- and ·OH. What is more, it showed that the ZVI/PS/Cu^{2+} system had a wider pH working range and had great potential to clean up heavy metal and organic compounds in running water and other

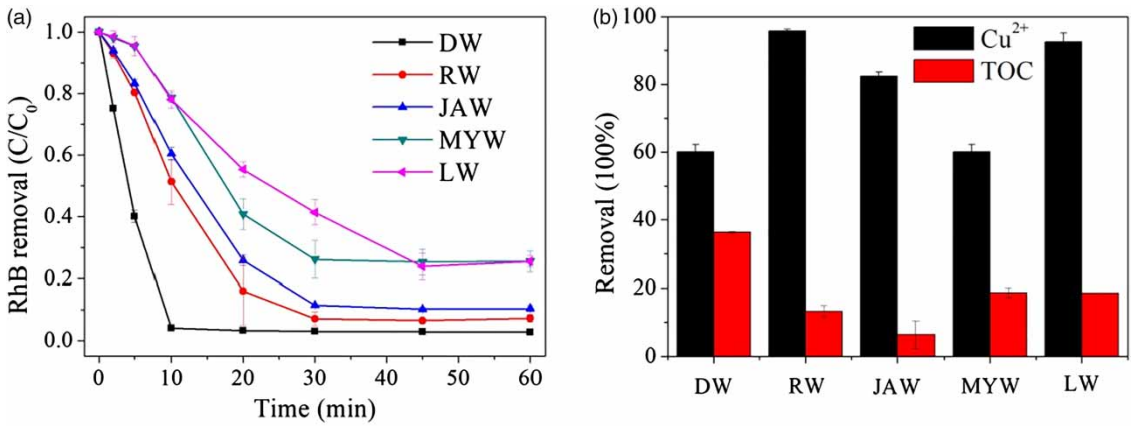

Figure 10 | Effect of simulated wastewater on removal of RhB (a) and Cu^{2+} (b) in the ZVI/PS/Cu^{2+} system ($[RhB]_0 = 20$ mg/L, $T = 25 \pm 1$ °C, $[ZVI]_0 = 100$ mg/L, $[PS]_0 = 1.0$ mM, $[Cu^{2+}]_0 = 0.2$ mM).

Table 2 | Characteristics of different water matrices

Water type	pH	TOC (mg/L)
DW	5.75 ± 0.01	0
RW	8.27 ± 0.01	1.85 ± 0.03
JAW	8.49 ± 0.01	2.99 ± 0.07
MYW	8.69 ± 0.01	6.41 ± 0.04
LW	8.65 ± 0.01	7.64 ± 0.11

realistic conditions based on the AOPs. Most importantly, the study confirmed the promise of the system for the simultaneous removal of heavy metal and organic compounds, which can be harnessed for the practical treatment of complicated water matrices.

ACKNOWLEDGEMENTS

This research did not receive any specific funding. We are grateful for the characterization examination test provided by 'Ceshigo' (www.ceshigo.com).

REFERENCES

Bilal, M., Asgher, M., Parra-Saldivar, R., Hu, H., Wang, W., Zhang, X. & Iqbal, H. M. N. 2017 Immobilized ligninolytic enzymes: an innovative and environmental responsive technology to tackle dye-based industrial pollutants – A review. *Science of the Total Environment* **576**, 646–659.

Doong, R. A., Tsai, C. W. & Liao, C. I. 2012 Coupled removal of bisphenol A and copper ion by titanate nanotubes fabricated at different calcination temperatures. *Separation & Purification Technology* **91** (19), 81–88.

Du, J., Bao, J., Lu, C. & Werner, D. 2016 Reductive sequestration of chromate by hierarchical FeS@Fe 0 particles. *Water Research* **102**, 73–81.

Fernandez, M. E., Nunell, G. V., Bonelli, P. R. & Cukierman, A. L. 2014 Activated carbon developed from orange peels: batch and dynamic competitive adsorption of basic dyes. *Industrial Crops & Products* **62** (62), 437–445.

Ferreira, R. A., Roma-Rodrigues, C., Davies, L. C., Sá-Correia, I. & Martins-Dias, S. 2016 A quantitative proteomic approach to highlight Phragmites sp. adaptation mechanisms to chemical stress induced by a textile dyeing pollutant. *Science of the Total Environment* **573**, 788–798.

Hu, L., Zhang, G., Meng, L., Qiao, W. & Peng, W. 2018 Enhanced degradation of Bisphenol A (BPA) by peroxymonosulfate with Co_3O_4-Bi_2O_3 catalyst activation: effects of pH, inorganic anions, and water matrix. *Chemical Engineering Journal* **338**, 300–310.

Li, R., Jin, X., Megharaj, M., Naidu, R. & Chen, Z. 2015 Heterogeneous Fenton oxidation of 2,4-dichlorophenol using iron-based nanoparticles and persulfate system. *Chemical Engineering Journal* **264**, 587–594.

Liang, C., Bruell, C. J., Marley, M. C. & Sperry, K. L. 2004 Persulfate oxidation for in situ remediation of TCE. I. Activated by ferrous ion with and without a persulfate–thiosulfate redox couple. *Chemosphere* **55** (9), 1213–1223.

Liang, C., Wang, Z. S. & Bruell, C. J. 2007 Influence of pH on persulfate oxidation of TCE at ambient temperatures. *Chemosphere* **66** (1), 106–113.

Lin, J., Ye, W., Zeng, H., Yang, H., Shen, J., Darvishmanesh, S., Luis, P., Sotto, A. & Bruggen, B. V. D. 2015 Fractionation of direct dyes and salts in aqueous solution using loose nanofiltration membranes. *Journal of Membrane Science* **477**, 183–193.

Liu, C. M., Diao, Z. H., Huo, W. Y., Kong, L. J. & Du, J. J. 2018 Simultaneous removal of Cu^{2+} and bisphenol A by a novel biochar-supported zero valent iron from aqueous solution: synthesis, reactivity and mechanism. *Environmental Pollution* **239**, 698–705.

Liu, Y., Zhou, P., Huo, X., Liu, Y., Cheng, X. & Zhang, Y. 2019 Pre-magnetization for enhancing the iron-catalyzed activation of peroxymonosulfate via accelerating the corrosion of Fe-0. *Water Science and Technology* **79** (7), 1287–1296.

Lü, Y., Li, J., Li, Y., Liang, L., Dong, H., Chen, K., Yao, C., Li, Z., Li, J. & Guan, X. 2019 The roles of pyrite for enhancing reductive removal of nitrobenzene by zero-valent iron. *Applied Catalysis B: Environmental* **242**, 9–18.

Mcelroy, W. J. & Waygood, S. J. 1990 Kinetics of the reactions of the SO^{-4} radical with SO–4, $S_2O_2^{-8}$, H_2O and Fe^{2+}. *Cheminform* **21** (44), 2557–2564.

Morshedi, D., Mohammadi, Z., Boojar, M. M. A., Aliakbari, F., Morshedi, D., Mohammadi, Z., Boojar, M. M. A. & Aliakbari, F. 2013 Using protein nanofibrils to remove azo dyes from aqueous solution by the coagulation process. *Colloids and Surfaces. B, Biointerfaces* **112** (12), 245–254.

Oh, W. D., Chang, V. W. C., Hu, Z. T., Goei, R. & Lim, T. T. 2017 Enhancing the catalytic activity of g-C_3N_4 through Me doping (Me = Cu, Co and Fe) for selective sulfathiazole degradation via redox-based advanced oxidation process. *Chemical Engineering Journal* **323**, 260–269.

Peng, G., Zhang, M., Deng, S., Shan, D., He, Q. & Yu, G. 2018 Adsorption and catalytic oxidation of pharmaceuticals by nitrogen-doped reduced graphene oxide/Fe_3O_4 nanocomposite. *Chemical Engineering Journal* **341**, 361–370.

Peng, G., Li, T., Ai, B., Yang, S., Fu, J., He, Q., Yu, G. & Deng, S. 2019 Highly efficient removal of enrofloxacin by magnetic montmorillonite via adsorption and persulfate oxidation. *Chemical Engineering Journal* **360**, 1119–1127.

Pulicharla, R., Drouinaud, R., Brar, S. K., Drogui, P., Proulx, F., Verma, M. & Rao, Y. S. 2018 Activation of persulfate by homogeneous and heterogeneous iron catalyst to degrade chlortetracycline in aqueous solution. *Chemosphere* **207**, 543–551.

Sharma, J., Mishra, I. M., Dionysiou, D. D. & Kumar, V. 2015 Oxidative removal of Bisphenol A by UV-C/peroxymonosulfate (PMS): kinetics, influence of co-existing chemicals and degradation pathway. *Chemical Engineering Journal* **276**, 193–204.

Triszcz, J. M., Porta, A. & Einschlag, F. S. G. 2009 Effect of operating conditions on iron corrosion rates in zero-valent iron systems for arsenic removal. *Chemical Engineering Journal* **150** (2–3), 431–439.

Vicente, F., Santos, A., Romero, A. & Rodriguez, S. 2011 Kinetic study of diuron oxidation and mineralization by persulphate: effects of temperature, oxidant concentration and iron dosage method. *Chemical Engineering Journal* **170** (1), 127–135.

Vigneswaran, S. 2006 Effluent organic matter (EfOM) in wastewater: constituents, effects, and treatment. *Critical Reviews in Environmental Science & Technology* **36** (4), 327–374.

Wei, C., Zhang, J., Zhang, Y., Zhang, G., Zhou, P., Li, W., Liang, J., Liu, Y. & Zhang, W. 2017 Ultrasound enhanced heterogeneous activation of peroxymonosulfate by a Co-NiOx catalyst. *Water Science & Technology* **76** (5–6), 1436–1446.

Wu, L., Liao, L., Lv, G., Qin, F., He, Y. & Wang, X. 2013 Micro-electrolysis of Cr (VI) in the nanoscale zero-valent iron loaded activated carbon. *Journal of Hazardous Materials* **254–255** (12), 277–283.

Yang, L., Guo, H., Zhang, Y., Tang, W., Xin, C. & Liu, H. 2016 Activation of peroxymonosulfate by $BiVO_4$ under visible light for degradation of Rhodamine B. *Chemical Physics Letters* **653**, 101–107.

Yueming, R., Xizhu, W. & Milin, Z. 2008 Adsorption character for removal Cu(II) by magnetic Cu(II) ion imprinted composite adsorbent. *Journal of Hazardous Materials* **158** (1), 14–22.

Zhou, L., Zheng, W., Ji, Y., Zhang, J., Zeng, C., Zhang, Y., Wang, Q. & Yang, X. 2013 Ferrous-activated persulfate oxidation of arsenic(III) and diuron in aquatic system. *Journal of Hazardous Materials* **263** (2), 422–430.

Zhou, P., Zhang, J., Zhang, Y., Zhang, G., Li, W., Wei, C., Liang, J., Liu, Y. & Shu, S. 2017 Degradation of 2,4-dichlorophenol by activating persulfate and peroxomonosulfate using micron or nanoscale zero-valent copper. *Journal of Hazardous Materials* **344**, 1209–1219.

First received 18 May 2019; accepted in revised form 14 July 2019. Available online 30 August 2019